Preprints.org

Article

Not peer-reviewed version

NaBH4-Mediated Co-Reduction Synthesis of Glutathione Stabilized Gold/Silver Nanoclusters for Detection of Magnesium Ions

Weiwei Chen , Yiying Chen , Xianhu Zhu , Miaomiao Xu , Zhihao Han , Lianhui Wang , Lixing Weng *

Posted Date: 17 July 2023

doi: 10.20944/preprints202307.1031.v1

Keywords: bimetallic AuAg nanoclusters; coordination; glutathione; NaBH4; magnesium ions

Article

$NaBH_4$-Mediated Co-Reduction Synthesis of Glutathione Stabilized Gold/Silver Nanoclusters for Detection of Magnesium Ions

Weiwei Chen [1], Yiying Chen [1], Xianhu Zhu [2], Miaomiao Xu [1], Zhihao Han [2], Lianhui Wang [2] and Lixing Weng [1,*]

[1] School of Geographic and Biologic Information, Nanjing University of Posts and Telecommunications, Nanjing 210023, China; chenww@njupt.edu.cn (W.C.); 2786222392@qq.com (Y.C.); xumiaomiao@njupt.edu.cn (M.X)

[2] State Key Laboratory for Organic Electronics and Information Displays, Jiangsu Key Laboratory for Biosensors, Institute of Advanced Materials (IAM), Jiangsu National Synergetic Innovation Center for Advanced Materials (SICAM), Nanjing University of Posts & Telecommunications, Nanjing 210023, China; 1221066727@njupt.edu.cn (X.Z.); 17698067082@163.com (Z.H.); iamlhwang@njupt.edu.cn (L.W.)

* Correspondence: lxweng@njupt.edu.cn

Abstract: The content of magnesium ions (Mg^{2+}) in drinking water is relatively high and the excessive Mg^{2+} ingestion may lead to pathological lesions in human body system. At present, the detection of Mg^{2+} still relies on costly devices or/and complex organic fluorescence probes. To solve this problem, this work proposed a $NaBH_4$-mediated co-reduction strategy for the synthesis of glutathione-stabilized bimetallic AuAg nanoclusters (GSH@AuAg NCs) with recognition performance to Mg^{2+}. The preparation of GSH@AuAg NCs was simple and rapid and could be performed at mild conditions. The reaction parameters and sampling orders were optimized to understand the formation mechanism of GSH@AuAg NCs. The GSH@AuAg NCs exhibited a sensitive "light-on" fluorescence response to Mg^{2+} due to the re-molding of the interfacial physicochemical environment following the Mg^{2+} coordination, which affected the surface charge transfer process, and thus led to a novel method for fluorescence detection of Mg^{2+} with admirable selectivity for Mg^{2+}. The proposed method showed a detection limit of 0.2 μM, and its practical utility for the detection of Mg^{2+} in real sample of purified drinking water was also demonstrated, confirming its practicability in monitoring the Mg^{2+} concentration in drinking water.

Keywords: bimetallic AuAg nanoclusters; coordination; glutathione; $NaBH_4$; magnesium ions

---

1. Introduction

Quantum-sized metal nanoclusters (MNCs) that only contain a few dozen atoms possess plenteous optical properties, such as outstanding fluorescence, size-dependent fluorescence, and ligand-tunable fluorescence, and thus hold great promise in fluorescent sensing applications [1–5]. Among MNCs, bio-liganded Au and Ag NCs prepared by easy one-pot synthesis has received the most attention due to their intrinsic luminescence properties [5–8]. To obtain the nanoclusters with superior stable and strong fluorescence, different bio-ligands such as peptides, proteins and DNA etc have been used as the protective shell to wrap the core of metal atoms [8–10]. Besides, glutathione (GSH, l-γ-glutamyl-l-cysteinyl-glycine) containing one thiol (-SH) and two carboxyl (-COOH) functional groups has been considered as the most adopted stabilizer since it can protect nanoclusters more efficiently [9,10]. However, GSH-capped Au and Ag NCs still exist some problems in practical applications, which are caused by low quantum yields (QYs) and less-than-perfect photon stability [10,11]. To solve these problems, some proteins with large cavity and abundant functional groups have been combined with GSH to act as protective ligands [11]. Extra efforts have also been invested in the preparation of Au/Ag bimetallic NCs (AuAg NCs). The Au and Ag can be easily mingled

Preprints (www.preprints.org) | NOT PEER-REVIEWED | Posted: 17 July 2023 doi:10.20944/preprints202307.1031.v1

without changing the lattice parameter of AuAg NCs due to their similar sizes to the Femi wavelength of an electron (0.7 nm). In addition, the interaction of Au and Ag can modify the electronic structure of alloy, surface composition, and deficiency, sharing distinct advantages of highly enhanced fluorescence and photon-stability over monometallic nanoclusters as the synergetic effect [11–13]. In this work a $NaBH_4$-mediated co-reduction strategy was proposed for the synthesis of GSH@AuAg NCs with excellent fluorescence properties.

To prepare GSH@AuAg NCs, an appropriate chemical environment must be provided to match the assembly of GSH ligand and Au and Ag precursors, which inevitably brings rigor reactive conditions such as strong alkali, high temperature, and prolonged reaction time [11,14]. Hence, there is a particular need to provide a simple and rapid method for GSH@AgAu NCs synthesis. Considering the mild conditions of $NaBH_4$ reduction for obtaining Au and Ag NCs [15], a one-pot synthesis method by simply mixing of certain proportion of $AuCl^{4-}$ and Ag^+ with GSH, and then $NaBH_4$ was developed (Scheme 1A), which could form GSH@AgAuNCs with strong fluorescent emission within a matter of minutes. Moreover, the GSH@AgAuNCs showed sensitive "turn-on" fluorescence response to magnesium ions (Mg^{2+}) (Scheme 1B), thus providing a simple method for Mg^{2+} detection.

Mg^{2+} is the most abundant intracellular divalent cation and plays a significant physiological role in numerous cellular processes [16]. Moreover, the excessive Mg^{2+} ingestion may lead to pathological lesions in cardiovascular, nervous, urinary, and hematopoietic [17,18]. However, most methods for detecting Mg^{2+} still needs expensive instrumentations, such as atomic absorption spectroscopy (AAS) and inductively coupled plasma-mass spectrometry (ICP-MS), and complex organic fluorescent probes [18–20]. It is valuable to design a simpler and more readily applicable sensor for Mg^{2+}. This work provided a mild and easy preparation method of GSH@AgAuNCs with admirable sensitivity and selectivity for fluorescent detection of Mg^{2+} ions. The practical utility of GSH@AgAuNCs in monitoring the Mg^{2+} in real sample of drinking water was also demonstrated.

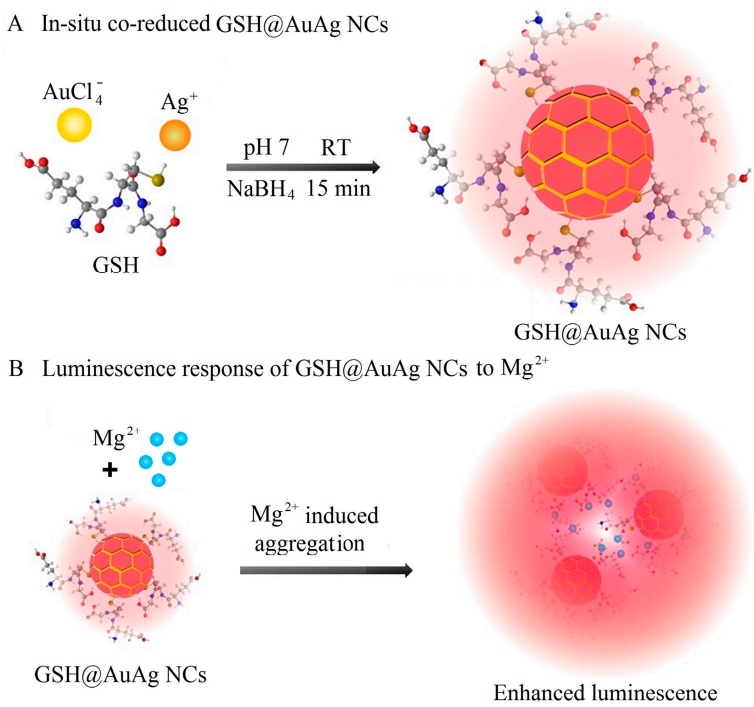

Scheme 1. Schematic illustration of (**A**) co-reduced synthesis of GSH@AuAg NCs and, (**B**) detection mechanism of Mg^{2+}.

Preprints (www.preprints.org) | NOT PEER-REVIEWED | Posted: 17 July 2023 doi:10.20944/preprints202307.1031.v1

2. Materials and Methods

2.1. Materials and Reagents

Silver nitrate ($AgNO_3$), glutathione (GSH), and sodium borohydride ($NaBH_4$) were purchased from Sigma-Aldrich (Shanghai). Chloroauric acid ($HAuCl_4$) was obtained from Energy Chemical Co., Ltd. Sodium hydroxide (NaOH) and other metal salts were products of Shanghai Aladdin Biochemical Technology Co., Ltd. Tyrosine (Try), arginine (Arg), lysine (Lys), proline (Pro), glycine (Gly), phenylalanine (Phe), histidine (His), aspartate (Asp), glucose (Glu), and cysteine (Cys). K^+, Na^+, Ca^{2+}, Mg^{2+}, Cr^{3+}, Cu^{2+}, Zn^{2+}, Ni^{2+}, Co^{2+}, Cd^{2+}, Mn^{2+}, Zr^{4+}, Al^{3+}, Fe^{2+} and Fe^{3+} solutions were prepared with KCl, NaCl, $CaCl_2{\cdot}2H_2O$, $MgCl_2$, $CrCl_3$, $CuCl_2{\cdot}2H_2O$, $ZnCl_2$, $NiSO_4{\cdot}6H_2O$, $CoCl_2{\cdot}6H_2O$, $CdCl_2{\cdot}5H_2O$, $MnCl_2{\cdot}4H_2O$, $AlCl_3{\cdot}6H_2O$, $FeSO_4{\cdot}7H_2O$ and $FeCl_3{\cdot}6H_2O$, respectively. All reagents were of analytical reagent grade and used as received without further purification. Ultrapure water with a resistivity of 18.2 $M\Omega{\cdot}cm^{-1}$ obtained from a Millipore purification system was used for the experiments.

2.2. Characterization

Fluorescence spectra were recorded on a FluoroMax Plus spectrophotometer (Shi madzu, Japan). The UV-vis-NIR absorption spectra were recorded on a UV-3600 spectrophotometer (Shimadzu, Japan). Transmission electron microscopic (TEM) images were collected with a JEM-2100 transmission electron microscope (JEOL Ltd., Japan). The morphologies and structures of GSH@AuAg NCs were characterized by high-resolution TEM (HRTEM) (FEI Talos F200X). Fluorescence lifetimes of GSH@AuAg NCs were collected by an Edinburgh FLS920 spectrofluorometer (Edinburgh, England). X-ray photoelectron spectroscopy (XPS) was performed on PHI 5000 VersaProbe with A1 Kα ($h\upsilon$ = 1486.6 eV) X-ray source (Ulvac-Phi, Japan).

2.3. Synthesis of GSH@AuAg NCs

Firstly, 50 μl $HAuCl_4$ (10 mM) was added to 758 μl ultrapure water in a 1.5 ml centrifuge tube, and mixed with 50 μl $AgNO_3$ (10 mM) to form flocculent precipitation. After stirring vigorously for 1 min, 50 μl GSH (20 mM) was added under vigorous stirring at room temperature for 5 min. 75 μl $NaBH_4$ (1 mM) dissolved in 0.25 M NaOH was then add to the mixture under ice water. Finally, 17 μl NaOH (0.25 M) was added to adjust the pH to 7.5. The GSH@AuAg NCs could be formed within 15 min at room temperature (25 ℃), which were washed using an Amicon Ultra-15 centrifugal filter with a molecular weight cutoff of 10 kDa (Merck Millipore, Billerica, USA), and then suspended in 1 ml of ultrapure water and reserved at 4 ℃.

2.4. Selective and Sensitive Detection of Mg^{2+}

After 100 μl GSH@AuAg NCs dispersion was diluted with 200 μl ultrapure water, and added with 5.0 μl Mg^{2+} solution or sample to incubate at room temperature for 5 min, the fluorescent emission spectrum was recorded at the excitation wavelength of 468 nm.

The selectivity of the proposed method was in terms of fluorescence intensity variation of GSH@AuAg NCs in the presence of metal ions (Mg^{2+}, Ca^{2+}, Na^+, K^+, Al^{3+}, Zr^{4+}, Zn^{2+}, Mn^{2+}, Cd^{2+}, Cr^{3+}, Fe^{2+}, Fe^{3+}, Co^{2+}, Ni^{2+}, Cu^{2+}). 100 μl GSH@AuAg NCs dispersion was diluted with 200 μl ultrapure water and then added with 50 μM metal ions (final concentration) to incubate at room temperature for 5 min, and the fluorescent emission spectra were recorded at the excitation wavelength of 468 nm.

3. Results and Discussion

3.1. Synthesis and Characterization of GSH@AuAg NCs

The reductant $NaBH_4$ was introduced in the mixture of $HAuCl_4$, $AgNO_3$ and GSH to accelerate the metallic nucleation and growth, which moderated the restricted synthesis conditions. After GSH@AuAg NCs were formed, the rate of $NaBH_4$ reduction was limited by harmonizing reaction parameters, such as solution pH, amounts of reactants, and temperature. Therefore, the reaction

Preprints (www.preprints.org) | NOT PEER-REVIEWED | Posted: 17 July 2023 doi:10.20944/preprints202307.1031.v1

conditions, such as the molar ratio of $HAuCl_4$ to $AgNO_3$ (Au/Ag), the concentrations of GSH and $NaBH_4$, and the pH were firstly optimized by detecting the fluorescence of produced GSH@AuAg NCs. The effect of Au/Ag ratio was examined in the presence of 0.5 mM $HAuCl_4$. The fluorescence intensity of GSH@AuAg NCs prepared at three pHs all increased gradually with the decreasing ratio of Au/Ag, and reached a maximum intensity at the molar ratio of 1:1 for pH 7-8 and 11-12, and 1:1.5 for pH 9-10 (Figure 1A-C). More $AgNO_3$ resulted in the decrease of fluorescence intensity of GSH@AuAg NCs and the appearance of a shoulder peak around 560 nm, which should result from other distinct clusters. The equal concentrations of Au and Ag precursors for the brightest nanoclusters hinted the co-doping of Au and Ag.

The effect of GSH ligand concentration was examined at different pHs with 0.5 mM Au and Ag precursors and 0.75 mM $NaBH_4$ to show the brightest GSH@AuAg NCs at 1.0 mM of GSH (Figure 1D-E). The GSH@AuAg NCs synthesized at pH 7-8 showed much stronger fluorescence intensity than those obtained at higher pHs. Thus pH 7.5 was selected for GSH@AuAg NCs synthesis.

The optimization of $NaBH_4$ concentration for GSH@AuAg NCs synthesis was performed at pH 7-8 with 0.5 mM Au and Ag precursors, and 1.0 mM GSH. The maximum fluorescence intensity occurred at 0.75 mM $NaBH_4$ (Figure S1 in SI). The optimized reaction time was 15 min, and prolonged reaction time did not increase the fluorescence intensity of GSH@AuAg NCs (Figure S2 in SI).

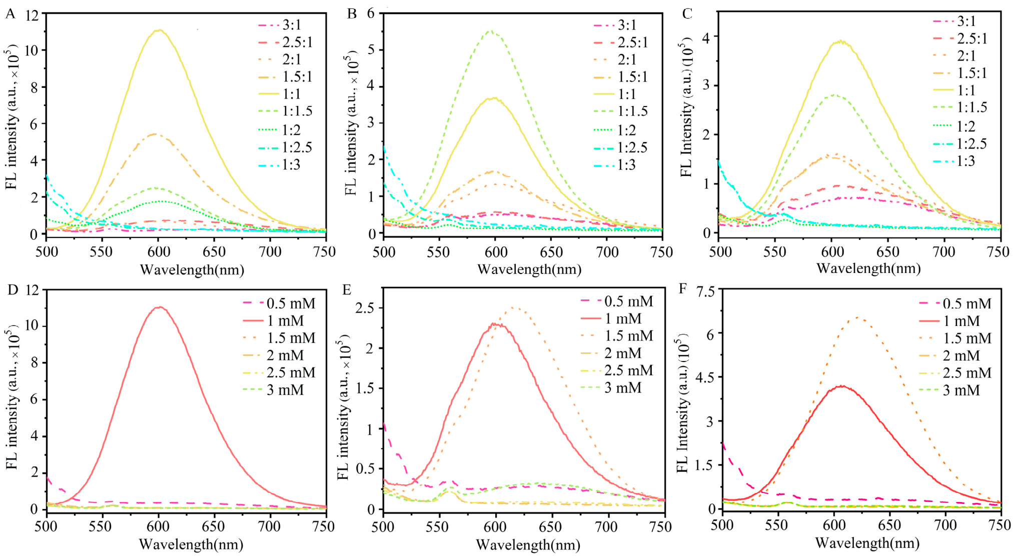

Figure 1. Condition optimization for GSH@AuAg NCs synthesis. (**A**-**C**) Molar ratio of Au to Ag at pH 7-8 (**A**), pH 9-10 (**B**) and pH 11-12 (**C**) in the presence of 0.5 mM Au, 1 mM GSH and 0.75 mM $NaBH_4$. (**D**-**F**) Concentration of GSH at pH 7-8 (**D**), pH 9-10 (**E**) and pH 11-12 (**F**) in the presence of 0.5 mM Au and Ag precursors, and 0.75 mM $NaBH_4$.

As the first reported co-reduction synthesis of GSH@AuAg NCs mediated by $NaBH_4$, the growth of GSH@AuAg NCs was investigated by UV-vis and fluorescence spectroscopy to understand the complex reduction assembly of Au and Ag precursors and GSH ligands. First, to confirm the doping synthesis of GSH@AuAg NCs rather than other luminous oligomeric clusters, spectroscopic analysis was performed by preparing the NCs in the absence of each reactant. The GSH@AuAg NCs did not exhibit obvious plasmon resonance absorption in the range of 400–700 nm, while a clear absorption peak appeared when the synthesis was performed in the absence of GSH or Au precursors (Figure 2A). In addition, in the absence of Ag precursor, the reaction solution was transparent and the UV-vis absorbance was close to zero, which was similar with that in the absence of $NaBH_4$ [Figure 2B, (3) and (5)], and could be attributed to the presence of GSH with two times higher concentration than $HAuCl_4$ to form stabilized Au (I)-GSH complexes, which limited the immediate reduction to Au (0) components [21,22]. In the absence of Au precursor, an absorption peak appeared at 450 nm and the solution became lilac color, which resulted from the formation of large Ag nanoparticles (AgNPs) [Figure 2B, (2)] due to the weaker stability of GSH and Ag^+ complexes. Interestingly, no fluorescence

Preprints (www.preprints.org) | NOT PEER-REVIEWED | Posted: 17 July 2023 doi:10.20944/preprints202307.1031.v1

emission was observed in the absence of Au or Ag precursor (Figure 2C), demonstrating that the fluorescence emission came from the bimetallic AuAg nanoclusters. In the absence of GSH a shield peak occurred at 560 nm [Figure 2C, curve (4)], as observed in (Figure 1), which eliminated the formation of the weak luminous metal (I)-GSH [M (I)-GSH] complexes. Besides, the mixture of Au and Ag precursors and GSH did not exhibit luminescence, which excluded the emission originating from oligomeric metal (I)-GSH complex. The above results confirmed that all reactants are indispensable for the formation of GSH@AuAg NCs.

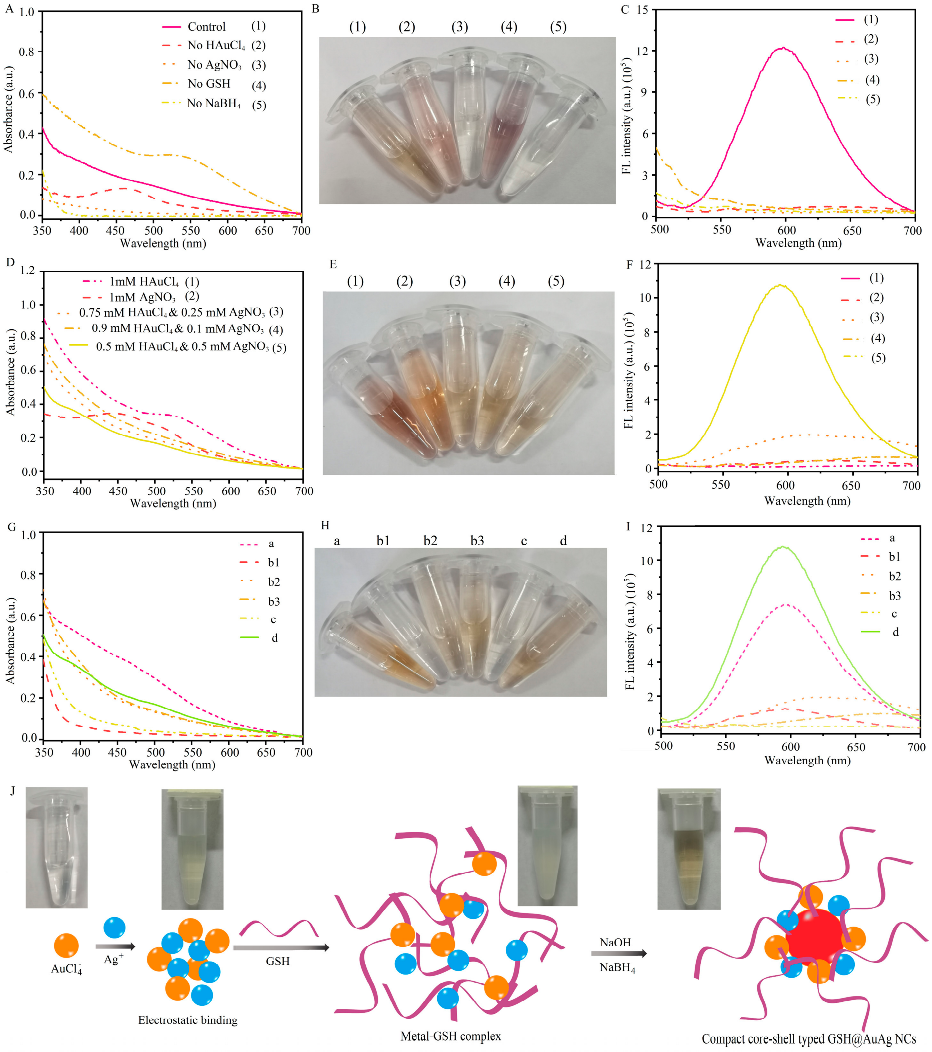

Figure 2. Growth process of GSH@AuAg NCs. (A,D,G) UV-vis absorption spectra, (**A**,**E**,**H**) photos and (**C**,**F**,**I**) FL spectra of the mixtures (1) 0.5 mM $HAuCl_4$, 0.5 mM $AgNO_3$, 1 mM GSH, and 0.75 mM $NaBH_4$ as control, and (2-5) (1) without presence of $HAuCl_4$ (2), $AgNO_3$ (3), GSH (4) and $NaBH_4$ (5) for (**A**,**B**,**C**); and 1 mM GSH, 0.75 mM $NaBH_4$ and (1) 1+0, (2) 0+1, (3) 0.75+0.25, (4) 0.9+0.1 and (5) 0.5+0.5 mM Au+ Ag precursors for (**D**,**E**,**F**); The reaction time is 15 min. (**G**-**I**) Effects of feeding orders: (a) pre-mixed GSH and Au precursor + Ag precursor and then $NaBH_4$, (b,c) pre-reduced Au (b) or Ag (c) precursor with $NaBH_4$ and GSH for 5 min + another precursor at (b1) 0.5 + 0.5, (b2) 0.75 + 0.25 and (b3) 0.9 + 0.1 mM Au + Ag precursors, (d) following the schematic order shown in (**J**).

To understand the interaction of Au and Ag precursors with GSH ligand, the ratio of GSH to Au precursor was changed while keeping the amount of GSH and total concentration of Au and Ag precursors at 1.0 mM to record the corresponding spectra. In the absence of Ag precursor, an absorption peak appeared at 520 nm, and the solution color turned deep reddish brown [Figure 2D and E, (1)], indicating the formation of Au NPs, and the above protective function of GSH only occurred at higher ratio of GSH to Au precursor. Interestingly, the absorption peak of Au NPs at 520

Preprints (www.preprints.org) | NOT PEER-REVIEWED | Posted: 17 July 2023 doi:10.20944/preprints202307.1031.v1

nm completely disappeared, and the solution became light brown-yellow after only 0.1 mM Ag precursor was added. More Ag precursor decreased the absorbance and solution color become lighter till the presence of 0.5 mM Ag precursor [Figure 2D and E, (3)-(5)]. The maximum fluorescence emission also occurred at 0.5 mM Au and Ag precursors (Figure 2F), demonstrating the synergism stability induced by co-doped Au and Ag and the formation of GSH@AuAg NCs.

The fluorescence of metal nanoclusters (MNCs) can be considered to originate from the aggregated M(I)-thiolate oligomers due to the formation of core-shell structure to induce ligand-to-metal charge transfer (LMCT) or ligand-metal-metal charge transfer (LMMCT) [21,22]. At high ratios of GSH to Au precursor, no Au (0) component was formed due to the protective effect of GSH ligand, thus the core-shell typed aggregates could not be generated. While introducing Ag to decentralize the shielding of GSH as forming M(I)–GSH complex, the $NaBH_4$ initially reduced the Ag (I) to Ag (0) as a less weak protection against reducing Ag (I) to Ag (0). As the intertwined M(I)–GSH complexes made the Au(I) ions close to the Ag (0) surface to prompt the formation of core-shell type bimetallic clusters [22].

To further understand the assembly of Au and Ag precursors and GSH ligand, the effect of the feeding pattern was examined to elucidate the formulation of GSH@AuAg NCs. The premixing of GSH ligand with Au precursor and later introduction of Ag precursor resulted in the growth of nanoclusters, which exhibited weaker luminosity and higher absorbance from 400 to 600 nm (Figure 2G-I, curve a), compared with the feeding mode that pre-mixed Au and Ag precursors, and then added GSH (Figure 2G-I, curve d), which showed the maximum luminosity, thus could be considered as an optimized sampling procedure (Figure 2J). In the optimized sampling procedure, the yellow mixture of Au and Ag precursors was attributed to the formation of multiple complexes by the electrostatic interaction, the solution became white muddy upon addition of GSH due to the formation of mingled network of Metal-GSH complex, and the addition of NaOH and $NaBH_4$ produced brown-yellow GSH@AuAg NCs.

Another sampling procedure was premixing GSH ligand with Au precursor and then $NaBH_4$ to react for 5 min, and then adding Ag precursor for another 10 min (Figure 2G-I, b). The absorbance of final solution was extremely low at 0.5 mM Au and Ag precursors (Figure 2G, curve b1), which was different from that of the optimized sampling order (Figure 2G, curve d). This demonstrated the influence of sampling order on the grow of GSH@AuAg NCs. In addition, further increasing the concentrations of Au precursor, both the color and absorption spectra of ultimate solution were close to that of the optimized sampling procedure, indicating the formation nanoclusters (Figure 2G, curves b2 and b3). These results confirmed the molar ratios of GSH to metal precursors significantly affected the assembly of Au, Ag and GSH. Other sampling procedure, such as premixing GSH ligand with Ag precursor, then $NaBH_4$ to react for 5 min and then adding Au precursor, was also examined (Figure 2G-I, c). After 5-min $NaBH_4$ reduction, the solution turned to lilac color, indicating the formation of large AgNPs as mentioned above. After introducing Au precursor (0.5 mM), the solution color gradually decayed to colorless, and the absorbance was also significantly reduced (Figure 2G and H, curve c), suggesting the dissolution of AgNPs due to the interaction among Au, Ag, and GSH. The significantly weak emission intensity demonstrated the failure of GSH@AuAg NCs assembly.

Both TEM and AFM images of GSH@AuAg NCs formed with the optimized sampling procedure showed spherical morphology and well dispersion with an average diameter of about 2.0±0.4 nm (Figure 3A-C). The clear lattice fringes were observed with an interspacing of 0.22 nm (inset in Figure 3B), corresponding to the d-spacing of the crystal plane of face-centered cubic Au (111) [23,24]. XPS spectroscopy was then used to confirm the elemental composition of the GSH@AuAg NCs and the valence states of Au and Ag (Figure 3D and E). The Au 4f XPS spectrum displayed a peak at 88.1 eV (Au $4f_{5/2}$) and a splitting peak at 84.4 eV (Au $4f_{7/2}$). The latter could be deconvoluted into two distinct components with the binding energies centered at 84.0 and 84.6 eV, assigned to Au (0) and Au (I), respectively. The predominant Au species in the GSH@AuAg NCs was identified as Au (I) (~62.5%). The Ag 3d pattern exhibited two peaks at 374.1 eV (Ag $3d_{3/2}$) and 368.1 eV (Ag $3d_{5/2}$), and the latter was deconvoluted into Ag (I) at 368.4 eV and Ag (0) at 367.7 eV (Figure 3E). The predominant Ag species in the GSH@AuAg NCs was identified as Ag (I) (~63.7%), indicating the successful doped

 doi:10.20944/preprints202307.1031.v1

synthesis of GSH@AuAg NCs [25,26]. GSH showed a FTIR peak ascribed to -SH stretching vibration at 2512 cm^{-1} [27], which disappeared in the spectrum of GSH@AuAg NCs (Figure 3F), while the FTIR peaks assigned to $-NH_2$ and -COOH groups at 1680, and 3383 cm^{-1} remained [28], demonstrating the binding of -SH with Au and Ag.

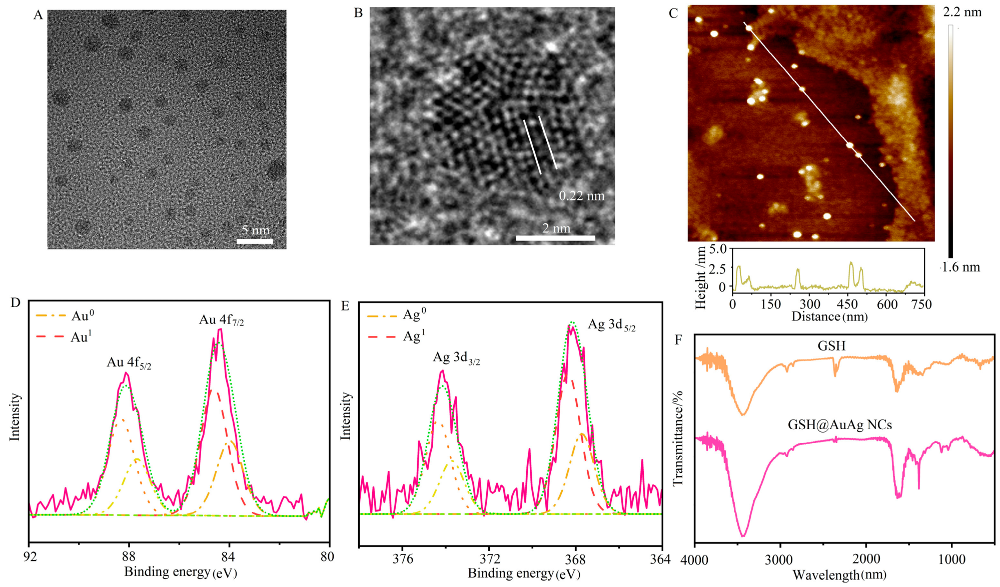

Figure 3. Characterization of GSH@AuAg NCs. (**A**) TEM, (**B**) HRTEM and (**C**) AFM images of GSH@AuAg NCs. (**D**) Au and (**E**) Ag XPS and (**F**) FTIR spectra of GSH@AuAg NCs.

3.2. Optimization of pH for Recognition of GSH@AuAg NCs to Mg^{2+}

MNCs, including AuAg NCs, have been reported to show fancy numerous responses to different metal ions [23,27,28]. To provide a new fluorescence probe for Mg^{2+}, the recognition conditions of GSH@AuAg NCs to Mg^{2+} were optimized. Firstly, the effect of pH on the fluorescence of GSH@AuAg NCs dispersion was examined (Figure 4A). The fluorescence was negligible at pHs lower than 6.5, and quickly enhanced with the increasing pH from 6.5 to 7.5 (Figure 4B). At different pHs the responses of GSH@AuAg NCs to several metal ions were also examined. As shown in Figure 4C, the fluorescence of GSH@AuAg NCs could be completely quenched by Cu^{2+} ions in the pH range of 6.0-10, while Mg^{2+} exhibited obvious boosting effect at different pHs. Besides, Ca^{2+} exhibited a relative weaker FL enhancement, and Zn^{2+} could quench the fluorescence at low pH and increase the fluorescence at pHs more than 9.0. Both Mg^{2+} and Ca^{2+} are the second main-group elements, and possess the similar coordinated interaction with GSH, leading to the FL enhancement. In order to achieve Mg^{2+} detection, the optimum pH was chosen at 7.5, at which the FL enhancement of Ca^{2+} was the weakest, and the effect of Zn^{2+} was also relatively low.

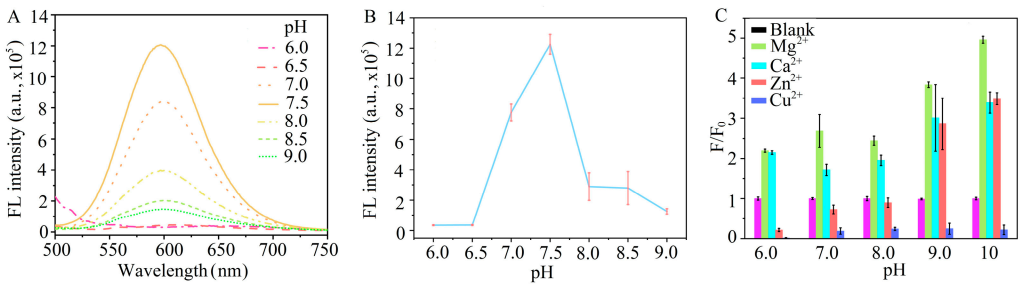

Figure 4. Effect of pH on FL response. (**A**) FL spectra and (**B**) intensity of GSH@AuAg NCs at different pHs. (**C**) FL responses to 50 μM metal ions.

Preprints (www.preprints.org) | NOT PEER-REVIEWED | Posted: 17 July 2023 doi:10.20944/preprints202307.1031.v1

3.3. Mechanism of Mg^{2+}-Mediated Fluorescence Enhancement of GSH@AuAg NCs

The TEM images of GSH@AuAg NCs showed the large aggregates with the size around 100 nm (Figure 5A), which was significantly larger than that of GSH@AuAg NCs (Figure 3), and could be attributed to the neutralization of negatively charged GSH@AuAg NCs by Mg^{2+} binding with $-COO^-$ in GSH and/or the chelation of Mg^{2+} to carbonyl, hydroxyl, and other electron-donating groups [29,30]. The neutralized GSH@AuAg NCs weakened the dispersal stability of the GSH@AuAg NCs due to the loss of electrostatic repulsion. The aggregates induced by the chelation of Mg^{2+} ion deeply changed the surface metal-ligand [Au (1)–GSH] motifs state, which remolded the ligand conformation and strengthened the aurophilic interaction of the oligomeric GSH–$[Au (I)–GSH]_x$ motifs [8,21,30].

To further understand the interaction of Mg^{2+} with GSH@AuAg NCs, the average fluorescent lifetime of GSH@AuAg NCs was examined upon addition of Mg^{2+} (Figure 5B). The fluorescent lifetime increased from 3.29 μs to 3.45 μs, while the fluorescent QY increased from 2.47 % to 7.16 % with the ethanol solution of rhodamine 6G as a reference. The large stokes shift (130 nm) and long fluorescence lifetime of GSH@AuAg NCs in their excited-state decay indicated that luminescence originated from the ligand-to-metal charge transfer (LMCT) or ligand-to-metal-metal charge transfer (LMMCT) [21,22]. The increase of fluorescent QY and the prolongation of fluorescent lifetime upon the addition of Mg^{2+} indicated the process of charge transfer underwent a transformation after Mg^{2+} chelation, further confirming the reconstructed local surface physicochemical environment.

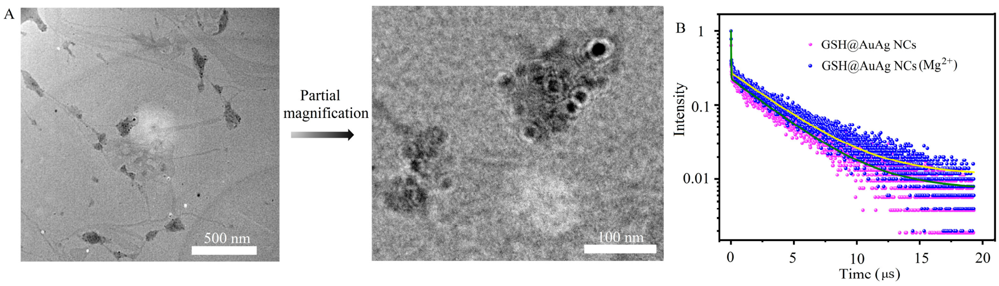

Figure 5. Mechanism of Mg^{2+}-induced FL enhancement. (**A**) TEM image of Mg^{2+}-induced aggregates of GSH@AuAg NCs. (**B**) FL lifetime of GSH@AuAg NCs before and after incubating with Mg^{2+}.

3.4. Sensing Performance towards Mg^{2+}

The emission intensity of GSH@AuAg NCs increased with the increasing Mg^{2+} concentration (Figure 6A). The plot of fluorescence intensity vs the concentration showed a good linearity with a R^2 of 0.989 over the range from 0.2 μM to 1 μM (Figure 6B). The linear regression equation was $F = 177 c (\mu M) + 3.848\times10^5$. In addition, other common metal ions except Ca^{2+} showed negligible effect on Mg^{2+} detection (Figure 6C). The fluorescence quenching of GSH@AuAg NCs by the coexisting ions did not affect the detection of Mg^{2+} (Figure 6D), demonstrating the admirable specificity of GSH@AuAg NCs towards Mg^{2+} and the potential application of the proposed method in the quality testing of Mg^{2+} amount.

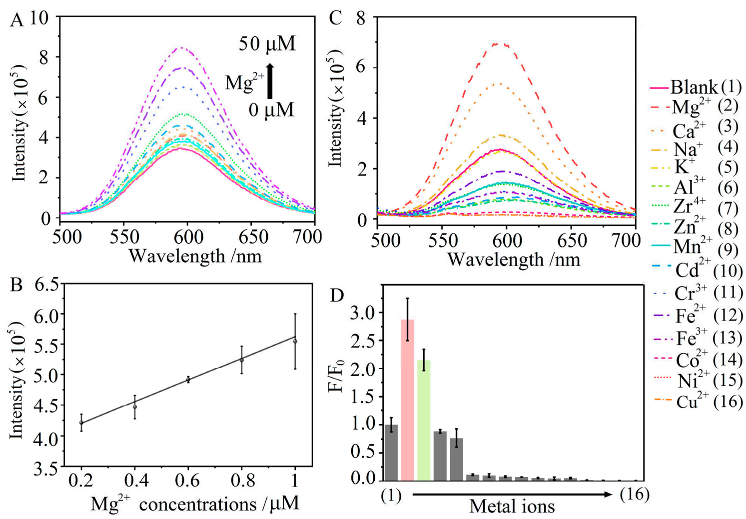

Figure 6. Sensing performance of GSH@AuAg NCs toward Mg^{2+}. (**A**) FL spectra of GSH@AuAg NCs after incubating with different concentrations of Mg^{2+}. (**B**) Plot of FL intensity of GSH@AuAg NCs vs Mg^{2+} concentration. (**C**) FL spectra of GSH@AuAg NCs after incubating with different metal ions. D) FL response of GSH@ AuAg NCs to different metal ions.

To demonstrate the practical analytical application of the GSH@AuAg NCs, Mg^{2+} was spiked into purified drinking water at different concentrations. Recovery results were presented in Table S1, which showed the recoveries ranging from 94.7% to 97.4%, indicating an applicable Mg^{2+} detection in real drinking water.

4. Conclusions

The facile, gentle, and fast synthesis of $NaBH_4$-reduced GSH@AuAg NCs with well dispersivity has been successfully achieved by pre-mixing Au and Ag precursors, and adding GSH in the mixture to form metal-GSH complex, followed with $NaBH_4$ addition for the reduction of metal ions at pH 7.5. The co-doping of Au and Ag at the molar ratio of 1:1 results in the synergism stability of the NCs. The GSH@AgAu NCs show a special enhancement of fluorescence response to magnesium ions (Mg^{2+}) at pH 7.0, which has been designed for the first nanoclusters-based fluorescent sensing of Mg^{2+}. The proposed method exhibits acceptable selectivity for Mg^{2+}detection, and practical utility in monitoring the Mg^{2+} content in daily drinking water.

Supplementary Materials: The following supporting information can be downloaded at the website of this paper posted on Preprints.org.

Author Contributions: Conceptualization, W.C.; methodology, W.C. and Y.C.; validation, Y.C., H.Z. and Z.H.; investigation, Y.C., H.Z. and Z.H.; resources, L.W. and L.W.; data curation, Y.C.; writing—original draft preparation, Y.C.; writing—review and editing, W.C., M.X. and L.W.; supervision, L.W.; funding acquisition, W.C. and L.W. All authors have read and agreed to the published version of the manuscript.

Funding: This research was financially supported by the National Natural Science Foundation of China (22004068), "the Belt and Road" Innovation Cooperation Project of Jiangsu (BZ2022011), the research fund from Nanjing University of Posts and Telecommunications (XK0320921144) and self-funding projects from State Key Laboratory of Analytical Chemistry for Life Science, Nanjing University (SKLACLS2207).

Institutional Review Board Statement: Not applicable.

Informed Consent Statement: Not applicable.

Data Availability Statement: Not applicable.

Conflicts of Interest: The authors declare no conflict of interest.

Preprints (www.preprints.org) | NOT PEER-REVIEWED | Posted: 17 July 2023 doi:10.20944/preprints202307.1031.v1

References

1. Yao, Q.; Chen, T.; Yuan, X.; Xie, J. Toward Total Synthesis of Thiolate-Protected Metal Nanoclusters. *Acc. Chem. Res.* **2018**, *51*, 1338-1348.
2. Jia, H.; Yu, S.; Yang, L.; Wei, Q.; Ju, H. Near-Infrared Electrochemiluminescence of Dual-Stabilizer-Capped Au Nanoclusters for Immunoassays. *ACS Appl. Nano Mater.* **2021**, *4*, 2657-2663.
3. Jia, H.; Yang, L.; Fan, D.; Kuang, X.; Sun, X.; Wei, Q.; Ju, H. Cobalt ion doping to improve electrochemiluminescence emisssion of gold nanoclusters for sensitive NIR biosensing. *Sens. Actuators B Chem.* **2022**, *367*, 132304.
4. Srinivasulu, Y.G.; Goswami, N.; Yao, Q.; Xie, J. High-Yield Synthesis of AIE-type Au22(SG)18 Nanoclusters through Precursors Engineering and Its pH-Dependent Size Transformation. *J. Phys. Chem. C* **2021**, *125*, 4066-4076.
5. Mastracco, P.; Gonzalez-Rosell, A.; Evans, J.; Bogdanov, P.; Copp, S.M. Chemistry-Informed Machine Learning Enables Discovery of DNA-Stabilized Silver Nanoclusters with Near-Infrared Fluorescence. *ACS Nano* **2022**, *16*, 16322-16331.
6. Aires, A.; Sousaraei, A.; Moller, M.; Cabanillas-Gonzalez, J.; Cortajarena, A.L. Boosting the Photoluminescent Properties of Protein-Stabilized Gold Nanoclusters through Protein Engineering. *Nano Lett* **2021**, *21*, 9347-9353.
7. Li, J.; Peng G.; Yu, Y.; Lin B.; Zhang, L.; Guo, M.; Cao, Y.; Wang Y. Cu^{2+}-mediated turn-on fluorescence biosensor based on DNA-templated silver nanoclusters for label-free and sensitive detection of adenosine triphosphate. *Microchim. Acta* **2023**, *190*, 41.
8. Zanetti-Polzi, L.; Charchar, P.; Yarovsky, I.; Corni, S. Origins of the pH-Responsive Photoluminescence of Peptide-Functionalized Au Nanoclusters. *ACS Nano* **2022**, *16*, 20129-20140.
9. Li X.; Luo J.; Jiang X.; Yang M.; Rasooly A. Gold nanocluster-europium(III) ratiometric fluorescence assay for dipicolinic acid. *Microchim. Acta* **2021**, *188*, 26.
10. Mi, W.; Tang, S.; Guo, S.; Li, H.; Shao, N. In situ synthesis of red fluorescent gold nanoclusters with enzyme-like activity for oxidative stress amplification in chemodynamic therapy. *Chinese Chem. Lett.* **2022**, *33*, 1331-1336.
11. Mi, W.; Tang, S.; Jin, Y.; Shao, N. Au/Ag Bimetallic Nanoclusters Stabilized by Glutathione and Lysozyme for Ratiometric Sensing of H_2O_2 and Hydroxyl Radicals. *ACS Appl. Nano Mater.* **2021**, *4*, 1586-1595.
12. Yin, M-M.; Chen, W-Q.; Hu, Y-J.; Liu, Y, Jiang, F-L. Rapid preparation of water-soluble Ag@Au nanoclusters with bright deep-red emission. *Chem. Commun.* **2022**, *58*, 2492-2495.
13. Cui, L.; Li, C.; Chen, B.; Huang H.; Xia, Q.; Li, X.; Shen Z.; Ge Z.; Wang, Y. Surface functionalized red fluorescent dual-metallic Au/Ag nanoclusters for endoplasmic reticulum imaging. *Microchim. Acta* **2022**, *187*, 66.
14. Li, Y.; Deng, Y.; Zhou, X.; Hu, J. A label-free turn-on-off fluorescent sensor for the sensitive detection of cysteine via blocking the Ag^{+}-enhancing glutathione-capped gold nanoclusters. *Talanta* **2018**, *179*, 742-752.
15. Farrag, M.; Tschurl, M.; Heiz, U. Chiral Gold and Silver Nanoclusters: Preparation, Size selection, and Chiroptical Properties. *Chem. Mater.* **2013**, *25*, 862-870.
16. Pontes, M.H.; Yeom, J.; Groisman, E.A. Reducing ribosome biosynthesis promotes translation during low Mg^{2+} stress. *Mol. Cell* **2016**, *64*, 480-492.
17. Kim, D. Y.; Shinde, S.; Ghodake, G. Colorimetric detection of magnesium (II) ions using tryptophan functionalized gold nanoparticles. *Sci. Rep.* **2017**, 7, 3966.
18. Li, L.; Ding, Y.; Zhang, C.; Xian, H.; Chen, S.; Dai, G.; Wang, X.; Ye, C. Ratiometric Fluorescence Detection of Mg^{2+} based on Regulating Crown-Ether Modified Annihilators for Triplet-Triplet Annihilation Upconversion. *J. Phys. Chem. B* **2022**, *126*, 3276-3282.
19. Gruskos, J. J.; Zhang, G.; Buccella, D. Visualizing Compartmentalized Cellular Mg^{2+} on Demand with Small-Molecule Fluorescent Sensors. *J. Am. Chem. Soc.* **2016**, *138*, 14639-14649.
20. Fujii, T.; Shindo, Y.; Hotta, K.; Citterio, D.; Nishiyama, S.; Suzuki, K.; Oka, K. Design and Synthesis of a FlAsH-Type Mg^{2+} Fluorescent Probe for Specific Protein Labeling. *J. Am. Chem. Soc.* **2014**, *136*, 2374-2381.
21. Goswami, N.; Yao, Q.; Luo, Z.; Li, J.; Chen, T.; Xie, J. Luminescent Metal Nanoclusters with Aggregation-Induced Emission. *J. Phys. Chem. Lett.* **2016**, *7*, 962-975.
22. Luo, Z.; Yuan, X.; Yu, Y.; Zhang, Q.; Leong, D.T.; Lee, J.Y.; Xie, J. From Aggregation-Induced Emission of Au(I)-Thiolate Complexes to Ultrabright Au (0) @Au (I)-Thiolate Core-Shell Nanoclusters. *J. Am. Chem. Soc.* **2012**, *134*, 16662-16670.
23. Wu, H.; Xie, R.; Hao, Y.; Pang, J.; Gao, H.; Qu, F.; Tian, M.; Guo, C.; Mao, B.; Chai, F. Portable smartphone-integrated AuAg nanoclusters electrospun membranes for multivariate fluorescent sensing of Hg^{2+}, Cu^{2+} and L-histidine in water and food samples. *Food Chem.* **2023**, *418*, 135961.
24. Zhang, X-L.; Li, X.; Li, X-T.; Gao, Y.; Feng, F.; Yang, G-J. Electrochemiluminescence sensor for pentoxifylline detection using Au nanoclusters@graphene quantum dots as an amplified electrochemiluminescence luminophore. *Sens. Actuators B Chem.* **2019**, *282*, 927-935.

 doi:10.20944/preprints202307.1031.v1

25. Jia, H.; Yang, L.; Dong, X.; Zhou, L.; Wei, Q.; Ju, H. Cysteine Modification of Glutathione-Stabilized Au Nanoclusters to Red-Shift and Enhance the Electrochemiluminescence for Sensitive Bioanalysis. *Anal. Chem.* **2022**, *94*, 2313-2320.
26. Zhang, B.; Chen, L.; Zhang, M.; Deng, C.; Yang X. A Gold-silver bimetallic nanocluster-based fluorescent probe for cysteine detection in milk and apple. *Spectrochim. Acta A: Mol. Biomol. Spectrosc.* **2022**, *278*, 121345.
27. Dong, W.; Yu, J.; Gong, X.; Liang, W.; Fan, L.; Dong, C. A turn-off-on near-infrared photoluminescence sensor for sequential detection of Fe^{3+} and ascorbic acid based on glutathione-capped gold nanoclusters. *Spectrochim. Acta A: Mol. Biomol. Spectrosc.* **2021**, *247*, 119085.
28. Zhao, R.; Liu A.; Wen, Q.; Wu, B.; Wang, J.; Hu, Y.; Pu, Z.; Ling J.; Cao, Q. Glutathione stabilized green-emission gold nanoclusters for selective detection of cobalt ion. *Spectrochim. Acta A: Mol. Biomol. Spectrosc.* **2021**, *254*, 119628.
29. Sadhanala, H.K.; Aryal, S.; Sharma, K.; Orpaz, Z.; Michaeli, S.; Gedanken, A. Nitrogen-doped carbon dots as a highly selective and sensitive fluorescent probe for sensing Mg^{2+} ions in aqueous solution, and their application in the detection and imaging of intracellular Mg^{2+} ions. *Sens. Actuators B Chem.* **2022**, *366*, 131958.
30. Chang, H.; Karan, N.S.; Shin K.; Bootharaju, M.S.; Nah, S.; Chae, S.I.; Baek, W.; Lee, S.; Kim, J.; Son, Y.J.; Kang T.; Ko, G.; Kwon, S-H.; Hyeon, T. Highly Fluorescent Gold Cluster Assembly. *J.Am. Chem. Soc.* **2021**, *143*, 326–334.